Commun Nonlinear Sci Numer Simulat 71 (2019) 118–129

Contents lists available at ScienceDirect

Commun Nonlinear Sci Numer Simulat

journal homepage: www.elsevier.com/locate/cnsns

Research paper

Multiscale interaction promotes chimera states in complex networks

Vladimir V. Makarov[a,b], Srilena Kundu[c], Daniil V. Kirsanov[a,b], Nikita S. Frolov[a,b], Vladimir A. Maksimenko[a,b], Dibakar Ghosh[c], Syamal K. Dana[d], Alexander E. Hramov[a,b,e,*]

[a] *REC "Artificial Intelligence Systems and Neurotechnology", Yuri Gagarin State Technical University of Saratov, 77 Politechnicheskaya str., Saratov 410054, Russia*
[b] *Department of Automation, Control, Mechatronics, Yuri Gagarin State Technical University of Saratov, 77 Politechnicheskaya str., Saratov 410054, Russia*
[c] *Physics and Applied Mathematics Unit, Indian Statistical Institute, Kolkata 700108, India*
[d] *Department of Mathematics, Jadavpur University, Kolkata 700032, India*
[e] *Saratov State University, 83 Astrakhanskaya str., Saratov 410012, Russia*

ARTICLE INFO

Article history:
Received 25 July 2018
Revised 28 October 2018
Accepted 21 November 2018
Available online 22 November 2018

Keywords:
Chimera state
Multiscale network
Mesoscopic interaction
Hindmarsh–Rose neurons

ABSTRACT

We report emergence of chimera states in a multiscale network that defines a network of interconnected networks, a network of a global ring of nodes whose each node, in turn, is a member of an individual subnetwork of another ring of nodes. We reveal a variety of spatiotemporal dynamics which ensues in such complex networks by varying the inner topology of the nonlocally coupled subnetworks from local to nonlocal coupling. We find that an increment in the local connectivity of the subnetworks enhances the span of the chimera region in parameter space. We consider the Kuramoto–Sakaguchi phase model to represent each node of the network and our numerical findings show that the topology of the subnetworks greatly influences the emergence of chimera states in the global ring. We also perform an analytical study on the phase oscillator based network using the Ott–Antonsen approach, and the analytical results are found to be consistent with the numerical outcomes. Furthermore, due to high relevance of the proposed network architecture to the human brain, we consider a more realistic network of Hindmarsh–Rose neuron model and reveal a similar phenomenon when the neurons in each of the subnetworks communicate via chemical synapses while information among the subnetworks passes through gap junctions.

1. Introduction

The processes arising on the frontiers of coherent and incoherent states in networks of dynamical units are of great interest in modern science. One of the emergent regimes is the familiar chimera states which is characterized by spatiotemporal pattern of coexisting coherent and incoherent groups of dynamical units. Such a strange pattern was first observed in 2002 by Kuramoto and Battogtokh [1] in a nonlocally coupled network of identical phase oscillators with an exponential coupling

* Corresponding author.
E-mail address: hramovae@gmail.com (A.E. Hramov).

https://doi.org/10.1016/j.cnsns.2018.11.015
1007-5704/

function, and later in 2004, a new terminology was coined to define the states as *Chimera states* by Abrams and Strogatz [2]. This distinctive nature of collective behavior has crucial importance in many real-world systems, such as the behavior of neuron ensembles. In contrast to normal sleep condition where both eyes are usually closed and both halves of the brain show reduced consciousness, during the unihemispheric slow-wave sleep [3,4], one half of the brain sleeps while the other half remains alert, which is observed in many marine mammals and migratory birds. As the neurons in the sleepy half of the brain are synchronized, the awake half remains desynchronized; this neural activity in the brain, in a sense, resembles the chimera states.

After the discovery of chimera states, it has attracted immediate attention of many researchers and so far, the studies reveal that such a symmetry breaking state not only emerges in networks with nonlocal coupling but also occurs in networks of oscillators under other coupling conditions [5], global (all-to-all) coupling [6–12] and local (nearest neighbor) coupling [13–16]. In fact, chimera states, by this time, is known to appear also in networks of limit-cycle oscillators [17,18], chaotic systems [19], time-delay systems [20,21] and neuronal systems [22,23] as well. Lately, attention has been paid to explore chimera states in networks of various complex topologies such as the heterogeneous networks [24], complex networks [25], time-varying [26], multiplexing networks [27–33] and modular networks [34]. Besides theoretical findings, there are remarkable experimental evidence of chimera states in chemical [35], mechanical [36], electronic [37,38], electrochemical [39] and laser [40] systems.

Several numerous studies also focuses on exploration of chimera patterns in networks of biological systems, namely, neuronal models, Fitzhugh–Nagumo model and Hindmarsh–Rose neuron model. Most of the earlier works [15,16,22,23] on chimera states in neuron models are concerned with nonlocally, locally, and globally coupled networks using both electrical and chemical synaptic interactions. However, recently, researchers aim to extend the chimera paradigm to more complex topologies. This includes the study of chimera states in multiplex neural network [27,28,31], modular neural network [34], two-dimensional lattice of neurons under local [41] and nonlocal [42] coupling, and bipartite neural network [43].

Nevertheless, there remains an open question *how chimera states emerge and exist in real networks, which are usually composed of a variety of interacting mesostructures?* Putting in another way, *how does chimera states reveal itself in a network of interconnected networks?* In nature, there are many networks, specifically some biological networks that are composed of a certain type of subnetworks with different inner and outer connectivity, i.e., different scales of topological structure, which can be referred to as multiscale networks. The cortical network in the human brain, being a very complex network, comprises of this type of multiscale structure [44,45]. Recently, the multiscale architecture of the human brain has become a feature of great interest among the researchers of the neuroscientific community. So it will be very meaningful to cast each node of the multiscale network by a neuron model and investigate the collective behavior of the network of subnetworks. A study on possible emergence of chimera states in such multiscale networks may give us interesting information, which can surely advance our knowledge in understanding the dynamics of interconnected networks.

We address the above question here with a study on a particular multiscale network, which is a network of subnetworks and where all the units are nonlocally coupled. Basically it is a nonlocally coupled global ring of oscillators where each node of the global ring is a member of another ring of locally or nonlocally coupled oscillators. We vary the inner topology of the subnetworks from local to nonlocal coupling and reveal a variety of collective dynamics. We first consider the Kuramoto–Sakaguchi (KS) phase oscillator to represent each node. This helped us to carry out an analytical treatment of the multiscale network by applying the Ott–Antonsen ansatz and verify our numerical results. Both the analytical and numerical results lead us to a conclusion that the topology of the subnetworks plays an important role on the emergence and stability of chimera states. An increase in the local connectivity of the subnetworks indeed induces the chimera states even in parameter regions, where it is absent in the case of simple nonlocally coupled ring. We check our results numerically in a more realistic network of Hindmarsh–Rose neurons where the neurons in the main global ring communicate via gap junctional pathway, and in the ring of subnetworks they are assumed communicating via chemical synapses.

The subsequent parts of this paper are organized as follows. Section 2 provides the formulation of the multiscale structure. Emergence of different dynamical states in the network of phase oscillators have been discussed here. Analytical results using the Ott–Antonsen ansatz are provided in Section 3. Section 4 is devoted to realistic network of Hindmarsh–Rose neurons. Finally, a conclusion of our findings is presented in Section 5.

2. Multiscale network: Kuramoto–Sakaguchi phase oscillator

The network under study is a global ring of M nonlocally coupled oscillators, each one of its node, in turn, is a member of a subnetwork that represents a nonlocally coupled ring of N oscillators as shown in a schematic diagram (Fig. 1). This represents a multiscale network structure where the subnetworks with coupling radii R_N act as units of the global ring of coupling radius R_M. Each node of the multiscale network is represented by the KS phase model, $\varphi_i^j(t)$ $(i = 1, 2, \dots N;\ j = 1, 2, \dots M)$ being the instantaneous phase of the system; M is the number of oscillators in the global ring, hence it is also the number of subnetworks, and N is the number of oscillators in each of these subnetworks. By this way, we form a network of networks with a fixed size of the global ring and its coupling radius, $M = 50$ and $R_M = 20,$ respectively.

Our first choice of dynamical system is motivated by the fact that the nonlocal interaction in a network of KS phase oscillators is a paradigm of chimera states [1,2] and it is solvable to the extent of the Ott–Antonsen analytical limit. The

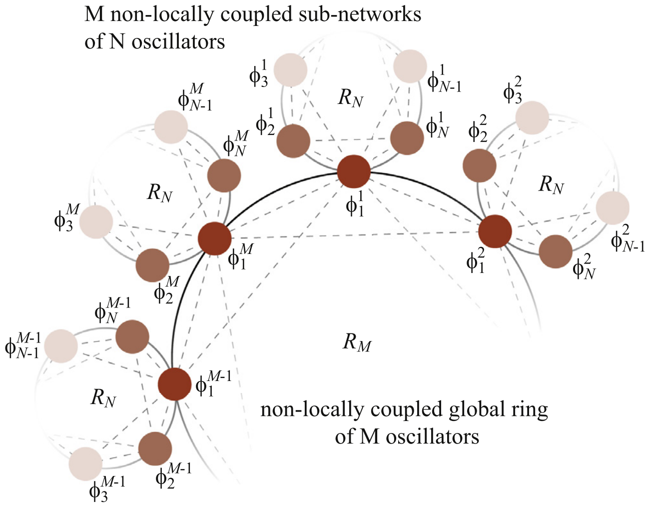

Fig. 1. Schematic diagram of a multiscale network whose node dynamics is governed by the phase oscillators φ_i^j. Here φ_i^j represents the i-th oscillator in the j-th subnetwork in a network of M subnetworks, each consisting of N nodes. Thus, each φ_i^j is located in the j-th ($j = 1, 2, \ldots, M$) coupled ring of N nodes with coupling radius R_N, which are connected among themselves through the nodes φ_1^j, forming a global ring of M nodes with coupling radius R_M. The dark red nodes (φ_1^j, $j = 1, 2, \ldots, M$) thus belong to two different types of network architecture, in this way forming a multiscale structure. (For interpretation of the references to color in this figure legend, the reader is referred to the web version of this article.)

phase dynamics of each node φ_i^j (ith node in the jth subnetwork) in the network is described by

$$\frac{d\varphi_i^j}{dt} = \begin{cases} \omega_i^j - \lambda \sum\limits_{k=i-R_N}^{i+R_N} \sin(\varphi_i^j - \varphi_k^j + \alpha), & i \neq 1, \\ \omega_i^j - \lambda \sum\limits_{k=i-R_N}^{i+R_N} \sin(\varphi_i^j - \varphi_k^j + \alpha) - \lambda \sum\limits_{k=j-R_M}^{j+R_M} \sin(\varphi_i^j - \varphi_i^k + \alpha), & i = 1. \end{cases} \tag{1}$$

where ω_i^j is the natural frequency of the ith oscillator in jth subnetwork, λ defines the coupling strength, which is same in all subnetworks as well as in the global ring. R_N and R_M are defined as the number of neighboring oscillators each oscillator is connected to, in both directions, in each subnetwork and the global ring, respectively; α is the phase lag parameter identical for all the oscillators and $\omega_i^j = 1.0$ for all oscillators in the network.

When all the subnetworks consist of only one node ($N = 1$) the system represents the classical nonlocally coupled global ring and demonstrates existence of chimera states when the value of α remains close to $\pi/2$ and for an appropriate choice of λ. The initial phase for oscillators in the global ring are the following,

$$\varphi_1^j(0) = \begin{cases} \pi\left(\frac{4j}{M} - 1\right), & j \in \left[0, \frac{M}{2}\right], \\ \pi\left(3 - \frac{4j}{M}\right), & j \in \left[\frac{M}{2} + 1, M\right]. \end{cases} \tag{2}$$

At the same time, when $N > 1$, the initial phase of oscillators in each subnetwork is identical,

$$\varphi_i^j(0) = \varphi_1^j(0) + \xi, \forall i, \tag{3}$$

where ξ is a small random fluctuation added for inhomogeneity.For a confirmation of the existence of chimera states in the global ring, we use a statistical measure, strength of incoherence SI [20], from a local standard deviation analysis. The SI is defined as

$$SI = 1 - \frac{\sum_{r=1}^{m} \Theta(\delta - \sigma_r)}{m}, \tag{4}$$

where $\Theta(\bullet)$ is the Heaviside step function, δ is a predefined threshold value, m is the number of bins of equal length $n = M/m$, for which the local standard deviation σ_r is calculated as

$$\sigma_r = \left\langle \sqrt{\frac{1}{n} \sum_{s=n(r-1)+1}^{rn} (\varphi_1^j - \Phi)^2} \right\rangle_t. \tag{5}$$

Here $\langle \bullet \rangle_t$ denotes averaging over time and Φ corresponds to the phase averaged over all the oscillators in the global ring. A value of $SI = 0$ represents a coherent state while $SI = 1$ and $0 < SI < 1$ represents incoherent and chimera states, respectively.

To reveal the degree of synchronization in both scales of the network, the global ring and the subnetwork, we calculate the classic order parameter for the global ring,

$$r_M = \frac{1}{M}\left|\sum_{j=1}^{M} e^{\varphi_1^j}\right|, \tag{6}$$

and an average order parameter for the subnetworks,

$$r_N = \frac{1}{M \times N}\sum_{j=1}^{M}\left|\sum_{i=1}^{N} e^{\varphi_i^j}\right|. \tag{7}$$

An examination of the r_M and r_N values allows us to get an insight of the interplay between the two different scales of the network and its influence on chimera patterns.

For a classical nonlocally coupled ring network of one scale, i.e., with only one node ($N = 1$) in each of the subnetworks, Fig. 2(a) shows a phase diagram of SI values in a parameter plane (α, λ). Chimera states emerge at $\lambda = 0.01$ and exists in a thin region of $\alpha \in [1.5;\ 1.57]$ that demonstrates almost no change while increasing λ. Fig. 2(d) reconfirm the existence of chimera states when the order parameter of the global ring, r_M, takes a value close to ≈ 0.7.

Next we extend the single scale network of one global ring to multiscale first by considering $N = 20$ and $R_N = 1$, when each oscillator of the global ring is also a member of a subnetwork of 20 locally coupled oscillators (Fig. 1), and (examine how such an extension of topology affect the span of chimera region in the parameter plane. The renewed phase diagrams of *SI*, order parameters r_M and r_N are shown in Fig. 2 (b, e, g), respectively. One can see that the chimera region expands largely, extending to the region with smaller values of phase lag. Similar to the $N = 1$ case, the global ring order parameter, r_M, demonstrates values close to 0.7 in all regions of the chimera states. On the contrary, the subnetworks' order parameter, r_N, is very small ($r_N \approx$ 0.1–0.2) in all points where λ is greater than 0.01 regardless of the dynamical regime. A small increase of its value can be seen during the transition to chimera states, and, then to the incoherent regime in the global ring. The extension of the chimera region can be considered as an evidence of competitive interaction between the global ring and the locally coupled group of subnetworks.

To prove this hypothesis we increase the connectivity of the subnetworks by increasing their coupling radius to $R_N = 5$. The corresponding plots are shown in the Fig. 2 (c, f, h). Here, the border between coherent and incoherent state is largely displaced to a lower α value near $\alpha = 1.2$. Nevertheless, the chimera region starts to demonstrate dependence on λ and becomes sufficiently less regular. A narrow chimera region appears at $\lambda = 0.005$ and continue to exist up to $\lambda = 0.025$, and then almost disappears at $\lambda = 0.03$. Let us now compare the values of r_M and r_N, the order parameters of the global ring and the subnetwork. At small values of phase lag, both scales of the network demonstrate high degree of synchronization. Increasing of α results in small, but sharp growth of r_N to full synchrony that is immediately followed by desynchronization of the global ring. Further increase of α causes the smooth decrease of order in subnetworks with a transition to incoherence ($\alpha \in [1.45;\ 1.65]$). Notably this region is also characterized by a small increase in the global order, r_M, that evidence a signature of the competitive interaction between the subnetworks and the global ring of oscillators.

Furthermore, we follow the dynamical regime while gradually increasing the number of nodes in the subnetworks, N, considering three values of coupling radius R_N. The corresponding dependency is shown in Fig. 3. First, we consider the case of locally coupled subnetworks ($R_N = 1$) and observe the strong influence of N on the width of the chimera region in Fig. 3(a). More specifically, increasing the subnetwork size (until $N = 10$) leads to a slight shifting of the chimera region to smaller values of α; in the range $N \in [10;\ 30]$, we observe a rapid growth of its width. In this range, the chimera region is reflected in the global ring by a slight decrease of $r_M \approx$ value to 0.6. A further increase of N leads to a fast narrowing of the chimera region and an almost vanish of the chimera region. Notably the subnetwork order parameter r_N does not reflect any correlation with the phase diagram or the values of an order in the global ring, r_M, demonstrating a rather irregular decrease with increasing of N.

Surprisingly, an increase of the coupling radius in the subnetworks to $R_N = 3$ (Fig. 3(b, e ,h)) have no qualitative effect on the phase diagram and on the global ring order parameter r_M accordingly. However, the subnetwork order parameter r_N starts to demonstrate more regular dependence with a sharp boundary between the high ($r_N \approx$ 0.7–0.85) and moderate ($r_N \approx$ 0.2–0.4) values. In a small region where $r_N \approx 1.0$ ($\alpha \approx 1.55$, $N \approx 7$) appears a dependence of r_M by the emergence of incoherent state in the global ring. This phenomenon is already seen in the Fig. 2 ($N = 20$, $R_N = 5$): a full synchrony in the subnetworks leads to desynchronization of the global ring. This effect is well-pronounced with a further increase in the coupling radius of the subnetworks ($R_N = 5$, Fig. 3(c, f, i)). The most of the chimera region is now occupied by the incoherent state provoked by complete synchronization in the subnetworks. We have already seen this transition in the Fig. 2 during the increase of R_N.

3. Ott–Antonsen reduction

Next we carry out an analytical study of KS oscillators to show the emergent chimera pattern in multiscale network of oscillators. We apply the Ott–Antonsen (OA) approach [46,47] to reduce the infinite-dimensional KS model to a system of finite dimensional differential equations. We rewrite Eq. (1) in a more compact form

$$\begin{aligned}\frac{d\varphi_i^j}{dt} &= \omega_i^j - \lambda \sum_{k=i-R_N}^{i+R_N} \sin(\varphi_i^j - \varphi_k^j + \alpha) \\ &-\delta_{i1}^j \lambda \sum_{k=j-R_M}^{j+R_M} \sin(\varphi_i^j - \varphi_i^k + \alpha)\end{aligned} \tag{8}$$

for $i = 1, 2, \ldots, N$; $j = 1, 2, \ldots, M$. Here δ_{i1}^j $(j = 1, 2, \ldots, M)$ is the Kronecker delta function which takes value 1 if $i = 1$ and 0 otherwise. Eq. (8) can be further reduced to get a simpler form,

$$\begin{aligned}&\dot{\varphi}_i^j = \omega_i^j - \frac{1}{2i}\left[r_i^j e^{i\varphi_i^j} - \bar{r}_i^j e^{-i\varphi_i^j}\right], \\ &\text{where } r_i^j = \lambda e^{i\alpha}\left[\sum_{k=i-R_N}^{i+R_N} e^{-i\varphi_k^j} + \delta_{i1}^j \sum_{k=j-R_M}^{j+R_M} e^{-i\varphi_i^k}\right].\end{aligned} \tag{9}$$

Considering the limit $M, N \to \infty$, we describe the dynamics of the network in terms of the probability density function $f(x, y, \varphi, t)$, defined for each of the oscillators, which satisfies the continuity equation

$$\frac{\partial f}{\partial t} + \frac{\partial (fv)}{\partial \varphi} = 0, \tag{10}$$

where v according to Eq. (9) is given by

$$v = \frac{d\varphi}{dt} = \omega - \frac{1}{2i}\left[re^{i\varphi} - \bar{r}e^{-i\varphi}\right], \tag{11}$$

the bar denotes complex conjugate and r is the order parameter which can be written as

$$\begin{aligned}r(x,y,t) &= \lambda e^{i\alpha}\left[\int_0^1 G_1(x-z,y)\int_0^{2\pi} f(z,y,\varphi,t)e^{-i\varphi}d\varphi dz\right. \\ &\left.+\int_0^1 \delta(x)G_2(x,y-z)\int_0^{2\pi} f(x,z,\varphi,t)e^{-i\varphi}d\varphi dz\right],\end{aligned} \tag{12}$$

where $G_1(x-z,y), G_2(x,y-z)$ are the subnetwork and global ring coupling kernels, respectively, given by,

$$\begin{aligned}G_1(x-z,y) &= \Theta[\cos((x-z)2\pi) - \cos(R'_N 2\pi)], \\ G_2(x,y-z) &= \Theta[\cos((y-z)2\pi) - \cos(R'_M 2\pi)],\end{aligned} \tag{13}$$

$R'_N = R_N/N$, $R'_M = R_M/M$ are normalized subnetwork and global coupling radii, respectively.

Next we attempt to find the solution $f(x, y, \varphi, t)$ in the form of Fourier series expansion considering the OA ansatz $f_n(x,y,\varphi,t) = a(x,y,t)^n$ in the following form,

$$f(x,y,\varphi,t) = \frac{1}{2\pi}\left(1 + \sum_{n=1}^{\infty}\left(a(x,y,t)^n e^{in\varphi} + \bar{a}(x,y,t)^n e^{-in\varphi}\right)\right). \tag{14}$$

Therefore,

$$\frac{\partial f}{\partial t} = \frac{1}{2\pi}\sum_{n=1}^{\infty}\left(na^{(n-1)}e^{in\varphi}\frac{\partial a}{\partial t} + n\bar{a}^{(n-1)}e^{-in\varphi}\frac{\partial \bar{a}}{\partial t}\right), \tag{15}$$

and

$$\begin{aligned}\frac{\partial (fv)}{\partial \varphi} &= f\frac{\partial v}{\partial \varphi} + v\frac{\partial f}{\partial \varphi} = \frac{1}{2\pi}\left(1 + \sum_{n=1}^{\infty}\left(a^n e^{in\varphi} + \bar{a}^n e^{-in\varphi}\right)\right) \\ &\times\left(-\frac{1}{2i}\left(rie^{i\varphi} + \bar{r}ie^{-i\varphi}\right)\right) + \left(\omega - \frac{1}{2i}\left(re^{i\varphi} - \bar{r}e^{-i\varphi}\right)\right) \\ &\times\left(\frac{1}{2\pi}\sum_{n=1}^{\infty}\left(a^n ine^{in\varphi} - \bar{a}^n ine^{-in\varphi}\right)\right)\end{aligned} \tag{16}$$

Substituting Eqs. (15) and (16) into Eq. (10) we obtain the following equation

$$\frac{\partial a}{\partial t} = -i\omega a + \frac{1}{2}(r - \bar{r}a^2), \tag{17}$$

where the order parameter with respect to the OA ansatz becomes

$$
\begin{aligned}
r(x,y,t) = \lambda e^{i\alpha}[&\int_0^1 G_1(x-z,y)a(z,y,t)dz \\
&+\int_0^1 \delta(x-\tfrac{1}{N})G_2(x,y-z)a(x,z,t)dz].
\end{aligned}
\tag{18}
$$

We substitute the OA ansatz $a=|a|e^{-i\psi}$ to Eq. (14) and obtain the phase distribution function as

$$
f(x,y,\varphi,t) = \frac{1}{2\pi}\frac{1-|a|^2}{(1-|a|^2)^2+2|a|[1-\cos(\varphi-\psi)]}. \tag{19}
$$

Here $|a|$ is the maximum value of the phase distribution $f(x, y, \varphi, t)$ and ψ is the phase value corresponding to the maximum distribution.

In particular, for any f given by Eq. (14), $a(x, y, t)$ can be written as

$$
a(x,y,t) = \int_0^{2\pi} f(x,y,\varphi,t)e^{i\varphi}d\varphi, \tag{20}
$$

which measures the degree of synchronization of the oscillators in the neighborhood of the point (x, y), thus it can be considered as a local order parameter. For any (x, y), $|a(x,y,t)|=1$ corresponds to the phase-locked state of the oscillator at position (x, y), i.e., the coherent motion. On the other hand $|a(x, y, t)|<1$ characterizes sparsely distributed phases or the incoherent motion of the oscillators.

Fig. 4(a, b, c) show the numerically simulated snapshots of the phase oscillators φ_1^j, situated on the global ring, for a particular choice of parameter values in the specified chimera regime of three distinct cases (as mentioned earlier). We also demonstrate the corresponding snapshots of the local order parameter $|a|$ in Fig. 4(d, e, f) by solving Eqs. (17) and (18) for an infinite number of oscillators. One can clearly see that $|a|$ takes a value 1 where the phase of the oscillators in the global ring are in coherent motion whereas $|a|<1$ for the oscillators in incoherent motion. Thus the analytical approach pretty well matches with the obtained numerical results.

4. Multiscale network: Hindmarsh–Rose neuron model

Next we explore the more realistic network of Hindmarsh–Rose (HR) neuron systems communicating through both electrical and chemical synapses. More specifically, our proposed multiscale network is structured in a global ring of M nonlocally coupled oscillators where information passes through electrical synapse or gap junctions and, in turn, each neuron in the global ring is a member of a subnetwork of N oscillators in an outer ring, which are communicating via chemical synapses. The network thus may be called as a hypernetwork [48] where a group of nodes interacts with another group of nodes via different type of interactions. There are evidence [49,50] that two forms of interneuronal communication (i.e., synapses) are active in the brain and essential for the normal brain function and its development. From this perspective, we formulate the multiscale network of the Hindmarsh–Rose system [16] using both the synaptic and electrical interactions,

$$
\begin{aligned}
\dot{x}_i^j &= \begin{cases}
a{x_i^j}^2 - {x_i^j}^3 - y_i^j - z_i^j + \\
+k_{ch}(v_s - x_i^j)\sum\limits_{k=i-R_N}^{i+R_N} C_{ik}^j\Gamma(x_k^j), & i\neq 1,\\
a{x_i^j}^2 - {x_i^j}^3 - y_i^j - z_i^j + \\
+k_{ch}(v_s - x_i^j)\sum\limits_{k=i-R_N}^{i+R_N} C_{ik}^j\Gamma(x_k^j) + k_{el}\sum\limits_{k=j-R_M}^{j+R_M} E(x_i^k, x_i^j), & i=1,
\end{cases}\\
\dot{y}_i^j &= (a+\alpha){x_i^j}^2 - y_i^j,\\
\dot{z}_i^j &= c(bx_i^j - z_i^j + e),
\end{aligned}
\tag{21}
$$

for $i=1,2,\dots,N,\ j=1,2,\dots,M$; N being the number of neurons in each of the M subnetworks. The transformed model, obtained after some linear transformations and parametric redefinitions [51] from the original model by Hindmarsh and Rose [52], is more simplified that can exhibit different types of bursting phenomena, observed in a number of biophysical models. The variables x_i^j represent the membrane potential, and y_i^j, z_i^j represent the transport of ions across the membranes through fast and slow channels respectively. The fast variable y_i^j measures the rate of change of the transport of sodium and potassium ions whereas the slow variable z_i^j measures the rate of change of transport of other ions. The speed of the slow variable z_i^j is controlled by the small parameter c such that z_i^j varies much slower than x_i^j and y_i^j. The neurons in the global ring are communicating through gap junctions (electrical synapse), whereas the neurons in each of the subnetworks are communicating via chemical synapses. The chemical synaptic coupling function is mathematically realized as a sigmoidal function $\Gamma(x)=\frac{1}{1+e^{-\kappa(x-\theta_s)}}$ where κ is the slope of the function, θ_s is the firing threshold, v_s is the reverse potential, and the electrical synaptic coupling function is realized by $E(x,y)=(x-y)$. Here we consider $v_s=2$ such that $v_s>x_i^j$ and the coupling is always excitatory, $\kappa=10$ and $\theta_s=-0.25$. The connectivity matrix $\mathcal{C}=\left(C_{ik}^j\right)_{N\times N}$ is such that $C_{ik}^j=1$, if the ith

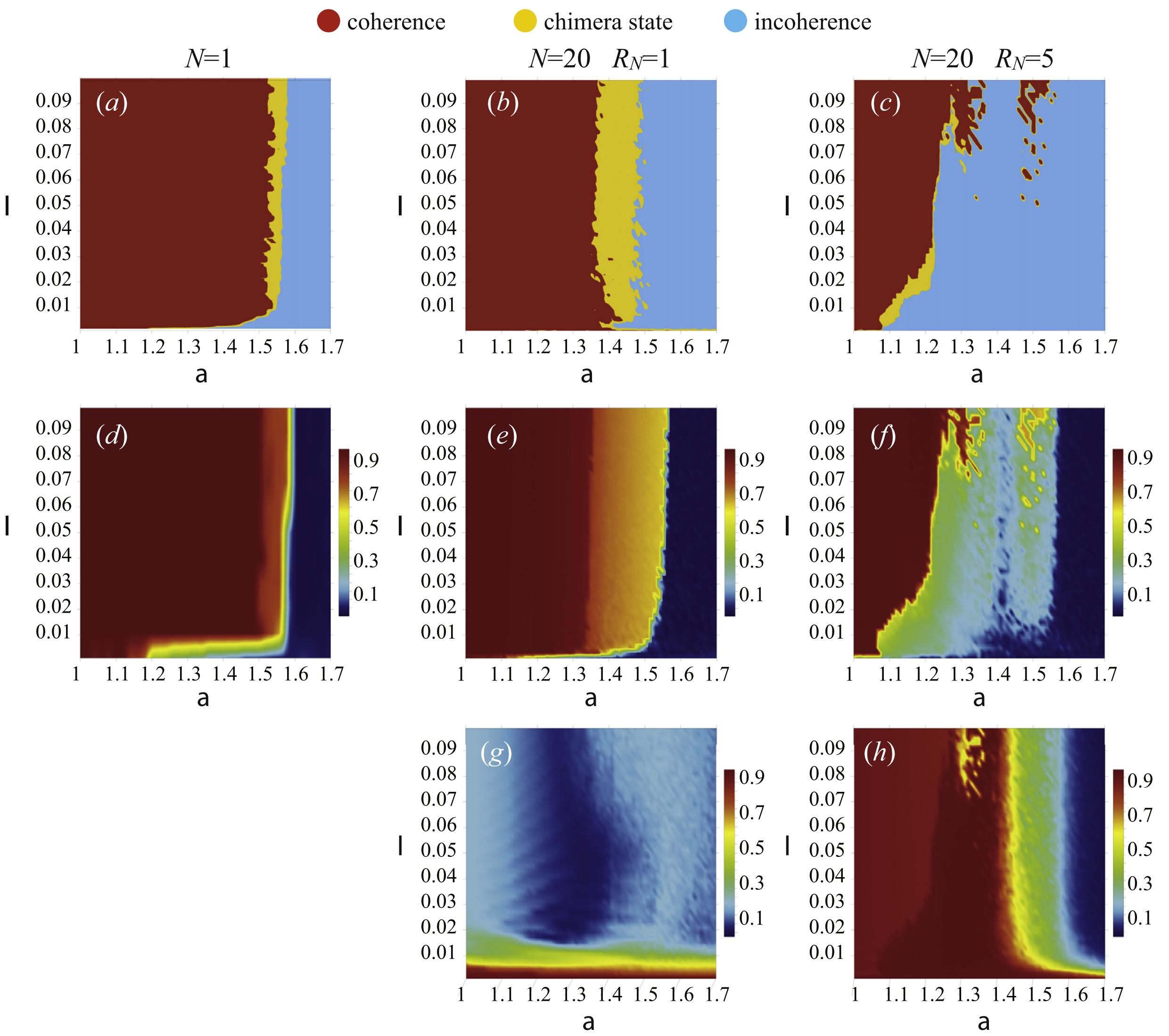

Fig. 2. Dynamical characteristics in the parameter space (λ, α) for various topologies of the subnetworks: (a, b ,c) dynamical regimes of oscillators in global ring (regimes markings are shown at the top of the figure), (d, e, f) r_M, order parameter, calculated for oscillators in global ring, (g, h) r_N, average order parameter calculated for oscillators in subnetworks. (a, d) $N = 1$ (i.e. only global ring exists), (b, e ,g) $N = 20$, locally coupled subnetworks, (c, f, h) $N = 20$, $R_N = 5$.

neuron is connected to kth neuron in the jth subnetwork, and 0 otherwise. k_{ch} and k_{el}, respectively, define the chemical and electrical synaptic coupling strength of the HR oscillators. As usual, R_M and R_N define the coupling range, in both directions, in each of the global ring and the subnetworks, respectively. The parameters of each HR model are chosen as $a = 2.8, \alpha = 1.6, c = 0.001, e = 5.0, b = 9.0$ so that the isolated system runs in the square wave bursting regime. We fix the number of neurons in the global ring and the coupling radius as $M = 40$ and $R_M = 10$, respectively.

We numerically simulate the multiscale network (21) by simultaneously varying the electrical and chemical synaptic coupling strengths k_{el} and k_{ch}, respectively, and using the fifth-order Runge-Kutta-Fehlberg algorithm, a time-step $dt = 0.01$ and a specific choice of initial conditions following Hindmarsh and Rose [52]. In case of $j \in [1, M/2]$, the initial conditions are:

$$x_1^j(0) = 0.01\left(j - \frac{M}{2}\right), y_1^j(0) = 0.02\left(j - \frac{M}{2}\right), z_1^j(0) = 0.03\left(j - \frac{M}{2}\right) \tag{22}$$

and for $j \in [M/2 + 1, M]$:

$$x_1^j(0) = 0.1\left(\frac{M}{2} - j\right), y_1^j(0) = 0.12\left(\frac{M}{2} - j\right), z_1^j(0) = 0.21\left(\frac{M}{2} - j\right). \tag{23}$$

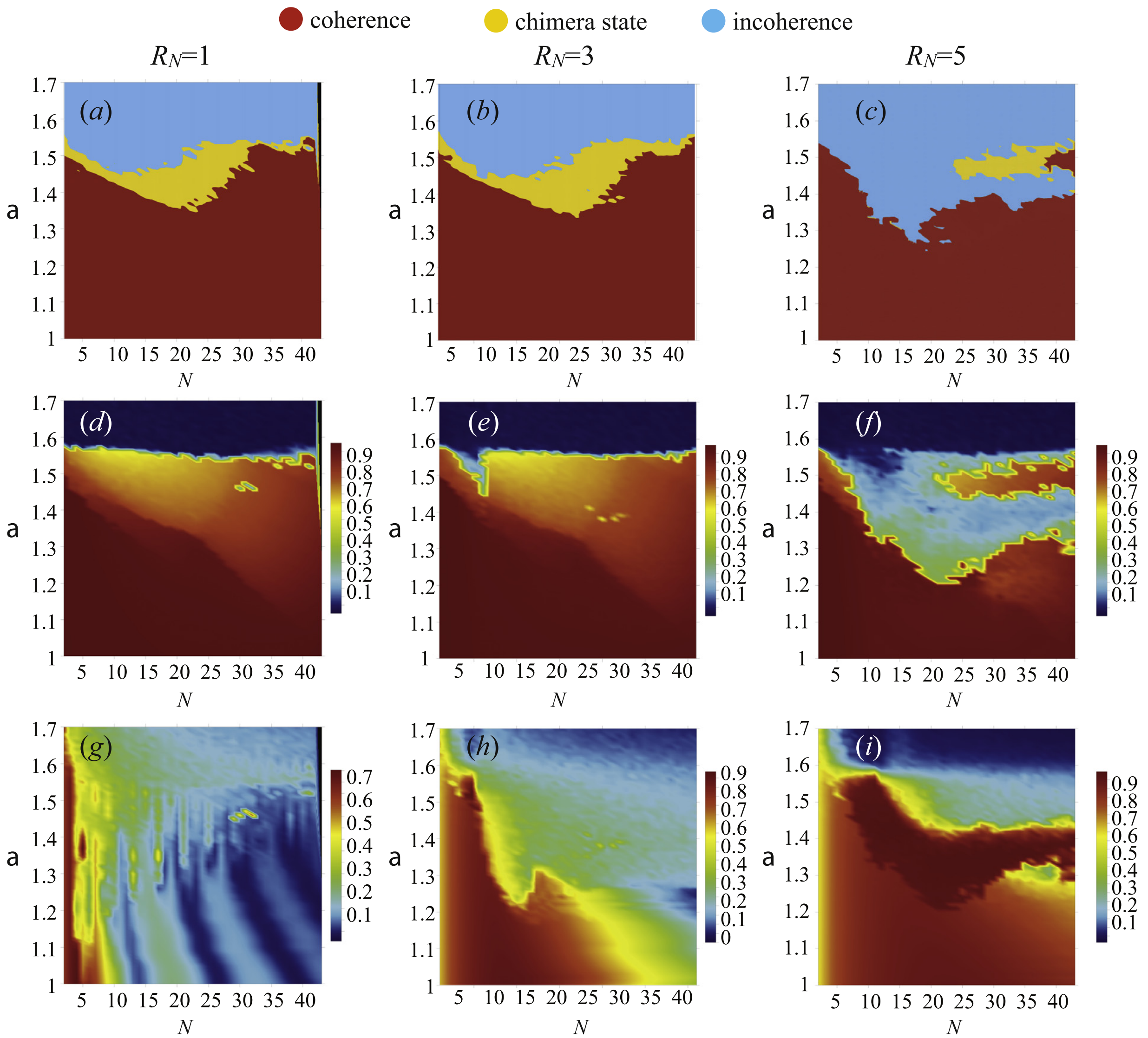

Fig. 3. Dynamical characteristics in the parameter space (α, N) for various coupling radius, R_N, of the subnetworks: (a, b, c) dynamical regimes of oscillators in global ring (regimes markings are shown at the top of the figure), (d, e, f) order parameter, calculated for oscillators in global ring, (g, h, i) average order parameter calculated for oscillators in subnetworks. The coupling strength $\lambda = 0.09$.

The initial states for the oscillators in each of the subnetworks is given by

$$x_i^j(0) = x_1^j(0) + \epsilon_i^j, y_i^j(0) = y_1^j(0) + \epsilon_i^j, z_i^j(0) = z_1^j(0) + \epsilon_i^j, \tag{24}$$

where ϵ_i^js are small random fluctuations added to the states for $i = 1, 2, \dots, N$; $j = 1, 2, \dots, M$.

Once again, we characterize the different dynamical regimes appearing in (k_{el}, k_{ch}) parameter plane of the oscillators in the global ring by using the SI measure Eq. (4). The degree of synchrony among the oscillators in the global ring as well as in the subnetworks, is determined using the following order parameters r_M and r_N, respectively,

$$r_M = \left\langle \frac{1}{M} \Big| \sum_{j=1}^{M} e^{i\phi_1^j(t)} \Big| \right\rangle_t,$$
$$r_N^j = \left\langle \frac{1}{N} \Big| \sum_{i=1}^{N} e^{i\phi_i^j(t)} \Big| \right\rangle_t, \tag{25}$$

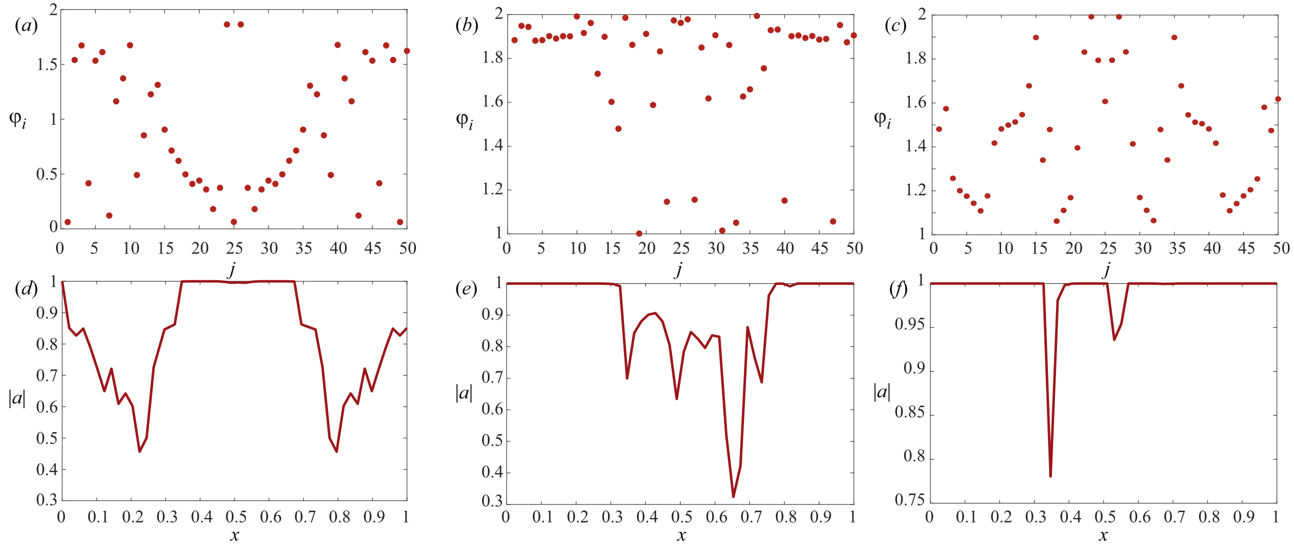

Fig. 4. The upper panel shows the snapshots of the phase distribution φ_1^j at a particular instant $t = 1600$, obtained by numerically solving Eq. (1) for three different cases as depicted in Fig. 2. The lower panel shows the corresponding snapshots of $|a|$. Plots (a,d) correspond to the consideration of the global ring in the absence of subnetworks with $N = 1$, $\alpha = 1.52$, $\lambda = 0.08$. Plots (b, e) illustrate chimera state in multiscale network in presence of subnetworks with a small subnetwork coupling radius $R'_N = 0.05$ and $\alpha = 1.4$, $\lambda = 0.05$ ($N = 20$ in numerical simulation). Plots (c, f) represent multiscale network state under the increase of subnetwork coupling radius $R'_N = 0.25$ and $\alpha = 1.22$, $\lambda = 0.03$ ($N = 20$ in numerical simulation). Here $M = 50$ is considered for the numerical simulation.

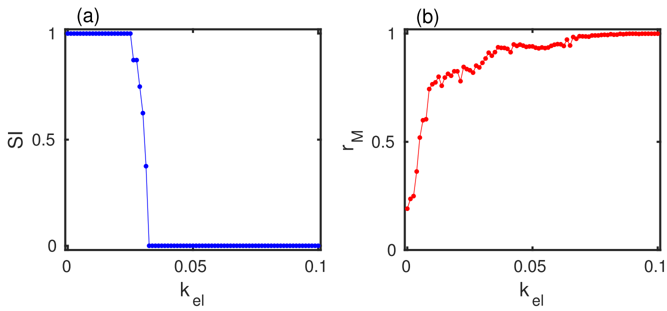

Fig. 5. (a) Strength of incoherence SI, and (b) order parameter r_M of oscillators in the nonlocally coupled ring corresponding to the coupling strength k_{el}, when the subnetworks consist of only one node i.e., $N = 1$. Here $M = 40, R_M = 10$ is fixed.

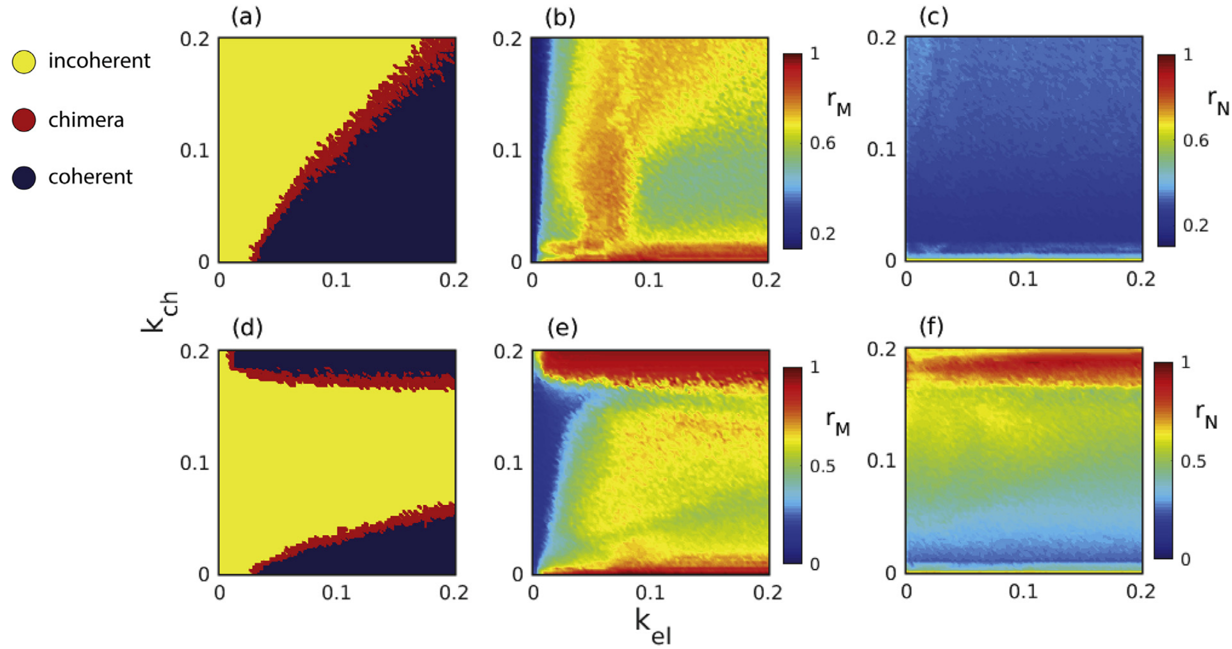

Fig. 6. (a,d) Phase diagram of the oscillators in the global ring using strength of incoherence (SI) measure. Yellow, red, and blue color corresponds to the incoherent, chimera and coherent regions, respectively. (b,e) Order parameter r_M of the oscillators in global ring, and (c,f) average order parameter r_N calculated for the oscillators in the subnetworks. The upper panel shows results for $N = 20, R_N = 1$ and the lower panel shows results for $N = 20, R_N = 3$. Here the number of subnetworks $M = 40$ and the coupling radius $R_M = 10$ is fixed and all the figures are plotted in (k_{el}, k_{ch}) parameter plane. (For interpretation of the references to color in this figure legend, the reader is referred to the web version of this article.)

where $\phi_i^j(t)$ represents the instantaneous phase of the ith neuron in the j–th subnetwork and is calculated using [53]

$$\phi_i^j(t) = \frac{2\pi(t - T_k)}{T_{k+1} - T_k}, \qquad T_k \le t \le T_{k+1}. \tag{26}$$

T_k is the time instant at which the kth peak occurs in a state variable. Thus $r_M, r_N \ll 1$ characterizes weak correlation or desynchronization among the neurons and r_M and $r_N \simeq 1$ characterize complete synchronization of the oscillators.

Fig. 5(a) shows a plot of SI in the nonlocally coupled global ring against the coupling strength k_{el} when the subnetworks consist of only one node ($N = 1$). Chimera states arise in a narrow window of $k_{el} \in [0.025, 0.035]$. The corresponding order parameter r_M in Fig. 5(b) shows that, for $k_{el} \ge 0.01$, it always remains larger than 0.75, and it becomes greater than 0.9 when the coherent region emerges at $k_{el} = 0.035$. Finally, for $k_{el} \ge 0.075$, r_M takes values almost equal to 1, which indicates a complete synchronized state.

Fig. 6(a,b,c) shows three phase diagrams using respective SI value of the oscillators in the global ring, global ring order parameter r_M, and average order parameter r_N of the subnetworks, respectively, in the (k_{el}, k_{ch}) parameter plane. The number of oscillators in each of the subnetworks is $N = 20$ and the coupling radius $R_N = 1$. Different regimes, the incoherent, chimera and coherent regions are indicated by yellow, red and blue colors, respectively. It is visible from Fig. 6(a) that chimera states emerge above a certain value of k_{el} and it spreads over the parameter region slowly with the simultaneous increment of two coupling strengths k_{el} and k_{ch}. Chimera region starts to appear at $k_{el} = 0.025$ and grows almost diagonally around the line $k_{el} = k_{ch}$ with the increase of both the synaptic strengths k_{el} and k_{ch}, dividing the whole parameter space into incoherent region (where $k_{ch} > k_{el}$ approximately) and coherent region (where $k_{el} > k_{ch}$ approximately). The corresponding order parameter r_M in Fig. 6(b) does not show any significant difference between the different dynamical regimes, though it remains high (> 0.5) almost everywhere except for $k_{el} < 0.02$, while the average subnetwork order parameter r_N takes lower values (< 0.3) except for $k_{ch} < 0.01$ as depicted in Fig. 6(c). This confirms a similar phenomenon as observed above in the multiscale network of phase oscillators, basically, reminding a competitive interaction between the non-locally coupled ring and the locally coupled subnetworks.

Next we increase the coupling radius of the subnetwork ($R_N = 3$), and plot the corresponding results in Fig. 6(d,e,f). Fig. 6(d) clearly visualizes that unlike the KS model, chimera states now emerge in two distinct regions in the parameter space, one for lower values of k_{ch} (cf. results with $R_N = 1$), and another for higher values of it, almost in whole range of k_{el}, which is different from the case of $R_N = 1$. Apparently it is discernible from the figure that the incoherent region enlarges and the coherent region diminishes in this case. The corresponding order parameter in Fig. 6(e) shows that the neurons in the upper coherent region are highly synchronous ($r_M \approx$ 0.9–0.94) rather than the neurons in the lower coherent region with order parameter $r_M \approx$ 0.65–0.8. In the upper chimera region the order parameter $r_M \approx$ 0.7–0.8, while in the lower chimera region the order parameter is much lower ($r_M \approx$ 0.53–0.55). The subnetwork order parameter r_N shows high degree of synchronization for larger values of k_{ch} in the upper coherent region of the global ring. But in the lower coherent region of the global ring the subnetwork order parameter r_N lies between $0.2 - 0.3$, which again can be thought of as an effect of competitive interaction between the global ring and the subnetworks. This also verifies our understanding of the fact that the connectivity of the subnetworks plays an important role in the emergence of chimera states in the global ring.

5. Conclusion

Emergence of a complex spatiotemporal pattern such as coexisting coherent and incoherent subpopulations of dynamical units, namely, the chimera states, has been one of the major interest among the researchers in diverse areas of science. Expectedly, this state has immense applicability in various neuronal functions, unihemispheric slow-wave sleep of some aquatic and avian species. They are suspected as greatly related to some brain diseases, such as Parkinsonâs disease, epileptic seizures, schizophrenia etc. In nature, there are many networks with complex architecture which may be composed of different scales of topologies and interaction, specifically, known as multiscale networks, and this type of multiscale architecture is highly relevant to the cortical network in the human brain.

In this paper, we have made an attempt to unravel different possible dynamical states, particularly, coherent, incoherent and chimera states arising in such a network of interconnected networks. For this, first, we have considered a multiscale network using the paradigmatic KS phase oscillator model for each node of the network. We have organized the multiscale structure as a network of nonlocally coupled subnetworks such that the inner topology of the subnetworks varies from local to nonlocal coupling. By using a SI measure, we have characterized the different dynamical regimes emerging in the global ring of the network, and our findings show that the increase in local connectivity of the subnetworks can promote the chimera states in the parameter region where it was absent earlier in case of simple nonlocally coupled ring. We have supported our numerical results analytically by employing the Ott–Antonsen approach in the continuum limit. Lastly, we have observed a similar scenario of collective dynamics in a realistic network of Hindmarsh–Rose neuron model interacting via two different synapses. Here we have considered that information among the neurons in each of the subnetworks passes through chemical synapses while the subnetworks themselves communicate with each other via electrical synapses. The introduction of electrical synapses among the subnetworks stimulates the neurons of the global ring from desynchronized to synchronized square wave bursting regime, for very small values of the chemical synaptic strength. However, if the chemical synaptic strength increases the dynamics of the neurons changes from square wave bursting to plateu bursting and for higher values of both the synapses they remain in the synchronized plateu bursting regime in the considered parameter space. A simultaneous presence of two distinct interactions in the multiscale structure (as considered here) evolves a hypernetwork organization, which has extensive applicability from the neurobiological perspective [54].

Acknowledgements

This work has been supported by the Russian Science Foundation (Grant17-72-30003).

References

[1] Kuramoto Y, Battogtokh D. Nonlinear Phenom Complex Syst 2002;5:380.
[2] Abrams DM, Strogatz SH. Phys Rev Lett 2004;93:174102.
[3] Rattenborg NC, Amlaner CJ, Lima SL. Neurosci Biobehav Rev 2000;24:817.
[4] Rattenborg NC. Naturwissenschaften 2006;93:413.
[5] Bera BK, Majhi S, Ghosh D, Perc M. Europhys Letts 2017;118:10001.
[6] Yeldesbay A, Pikovsky A, Rosenblum M. Phys Rev Lett 2014;112:144103.
[7] Chandrasekar VK, Gopal R, Venkatesan A, Lakshmanan M. Phys Rev E 2014;90:062913.
[8] Mishra A, Hens C, Bose M, Roy PK, Dana SK. Phys Rev E 2015;92:062920.
[9] Sethia GC, Sen A. Phys Rev Lett 2014;112:144101.
[10] Böhm F, Zakharova A, Schöll E, Lüdge K. Phys Rev E 2015;91:040901(R).
[11] Schmidt L, Krischer K. Phys Rev Lett 2015;114:034101.

[12] Schmidt L, Krischer K. Chaos 2015;25:064401.
[13] Hizanidis J, Lazarides N, Tsironis GP. Phys Rev E 2016;94:032219.
[14] Laing CR. Phys Rev E 2015;92:050904(R).
[15] Bera BK, Ghosh D. Phys Rev E 2016;93:052223.
[16] Bera BK, Ghosh D, Lakshmanan M. Phys Rev E 2016;93:012205.
[17] Ulonska S, Omelchenko I, Zakharova A, Schöll E. Chaos 2016;26:094825.
[18] Bera BK, Ghosh D, Parmananda P, Osipov GV, Dana SK. Chaos 2017;27:073108.
[19] Gu C, St-Yves G, Davidsen J. Phys Rev Lett 2013;111:134101.
[20] Gopal R, Chandrasekar VK, Venkatesan A, Lakshmanan M. Phys Rev E 2014;89:052914.
[21] Rakshit S, Bera BK, Perc M, Ghosh D. Sci Rep 2017;7:2412.
[22] Hizanidis J, Kanas V, Bezerianos A, Bountis T, Bifurcat J. Int Chaos 2014;24:1450030.
[23] Bera BK, Ghosh D, Banerjee T. Phys Rev E 2016;94:012215.
[24] Laing CR. Chaos 2009;19:013113.
[25] Zhu Y, Zheng Z, Yang J. Phys Rev E 2014;89:022914.
[26] Buscarino A, Frasca M, Gambuzza LV, Hövel P. Phys Rev E 2015;91:022817.
[27] Majhi S, Perc M, Ghosh D. Sci Rep 2016;6:39033.
[28] Maksimenko VA, Makarov VV, Bera BK, Ghosh D, Dana SK, Goremyko MV, Frolov NS, Koronovskii AA, Hramov AE. Phys Rev E 2016;94:052205.
[29] Ghosh S, Jalan S, Bifur J. Int Chaos 2016;26:1650120.
[30] Ghosh S, Kumar A, Zakharova A, Jalan S. Europhys Lett 2016;115:60005.
[31] Majhi S, Perc M, Ghosh D. Chaos 2017;27:073109.
[32] Makarov VV, Hramov AE, Kirsanov DV, Maksimenko VA, Goremyko MV, Ivanov AV, Yashkov IA, Boccaletti S. Sci Rep 2017;7:17246.
[33] Frolov NS, Maksimenko VA, Makarov VV, Kirsanov DV, Hramov AE, Kurths J. Phys Rev E 2018;98:022320.
[34] Hizanidis J, Kouvaris NE, Zamora-López G, Díaz-Guilera A, Antonopoulos CG. Sci Rep 2016;6:19845.
[35] Tinsley MR, Nkomo S, Showalter K. Nat Phys 2012;8:662.
[36] Martens EA, Thutupalli S, Fourriere A, Hallatschek O. Proc Natl Acad Sci USA 2013;110:10563.
[37] Larger L, Penkovsky B, Maistrenko Y. Phys Rev Lett 2013;111:054103.
[38] Gambuzza LV, Buscarino A, Chessari S, Fortuna L, Meucci R, Frasca M. Phys Rev E 2014;90:032905.
[39] Wickramasinghe M, Kiss IZ. PLoS ONE 2013;8:e80586.
[40] Larger L, Penkovsky B, Maistrenko Y. Nat Commun 2015;6:7752.
[41] Kundu S, Majhi S, Bera BK, Ghosh D, Lakshmanan M. Phys Rev E 2018;97:022201.
[42] Schmidt A, Kasimatis T, Hizanidis J, Provata A, Hövel P. Phys Rev E 2017;95:032224.
[43] Wu ZM, Cheng HY, Feng Y, Li HH, Dai QL, Yang JZ. Front Phys 2018;13:130503.
[44] Betzel RF, Bassett DS. Neuroimage 2017;160:73.
[45] Maksimenko VA, Runnova AE, Frolov NS, Makarov VV, Nedaivozov V, Koronovskii AA, Pisarchik A, Hramov AE. Phys Rev E 2018;97:052405.
[46] Ott E, Antonsen TM. Chaos 2008;18:037113.
[47] Ott E, Antonsen TM. Chaos 2009;19:023117.
[48] Sorrentino F. New J Phys 2012;14:033035.
[49] Pereda AE. Nat Rev Neurosci 2014;15:250.
[50] Rash JE, Dillman RK, Bilhartz BL, Duffy HS, Whalen LR, Yasumura T. Proc Natl Acad Sci USA 1996;93:4235.
[51] Belykh I, Hasler M. Patterns of synchrony in neuronal networks: the role of synaptic inputs. Nonlinear Dynamics: New Directions. New York: Springer; 2014.
[52] Hindmarsh JL, Rose M. Proc R Soc Lond Ser-B 1984;221:87.
[53] Liang X, Tang M, Dhamala M, Liu Z. Phys Rev E 2009;80:066202.
[54] Rakshit S, Bera BK, Ghosh D, Sinha S. Phys Rev E 2018;97:052304.